SUPPORTING INFORMATION

Hetero-hexa-lanthanide complexes: A new synthetic strategy for molecular thermometric probes.

Haiyun Yao, Guillaume Calvez*, Carole Daiguebonne*, Kevin Bernot, Yan Suffren and Olivier Guillou.

Univ Rennes, INSA Rennes, CNRS UMR 6226 "Institut des Sciences Chimiques de Rennes", F-35000 Rennes, France.

* To whom correspondence should be addressed

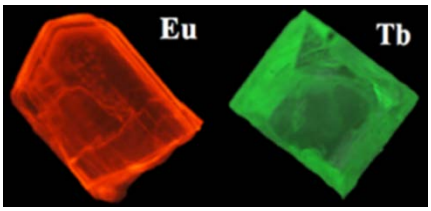

Figure S1. Pictures of $[Ln_6(3\text{-cb})_{14}]$ (Ln = Eu and Tb) under UV irradiation (λ_{exc} = 312 nm).

Table S1. Synthetic details of the syntheses of $[Ln_6(3\text{-cb})_{14}]$ and $[Ln_6(3\text{-bb})_{14}]$ (Ln = Eu-Tb)

Ln^{3+}	Temperature range (°C)	
	$[Ln_6(3\text{-cb})_{14}]$	$[Ln_6(3\text{-bb})_{14}]$
Eu^{3+}	60 - 70	60 - 70
Gd^{3+}	60 - 70	60 - 80
Tb^{3+}	60 - 80	80 - 100
Dy^{3+}	70 - 90	80 - 100

Table S2. Relative contents of Ln and Ln' for $[Y_{6x}Tb_{6-6x}(3\text{-cb/bb/ib})_{14}]$ complexes with $0 \leq x \leq 1$

	$[Y_{6x}Tb_{6-6x}(3\text{-cb})_{14}]$		$[Y_{6x}Tb_{6-6x}(3\text{-bb})_{14}]$		$[Y_{6x}Tb_{6-6x}(3\text{-ib})_{14}]$	
x^b	Tb^a(%)	Y^a(%)	Tb^a(%)	Y^a(%)	Tb^a(%)	Y^a(%)
0	100	0	100	0	100	0
0.05	94(2)	6(2)	93(2)	7(2)	94(2)	6(2)
0.1	88(2)	12(2)	87(2)	13(2)	87(2)	13(2)
0.2	78(2)	22(2)	76(2)	24(2)	79(2)	21(2)
0.5	47(2)	53(2)	49(2)	51(2)	50(2)	50(2)
0.7	26(2)	74(2)	-	-	-	-
0.9	8(2)	92(2)	9(2)	91(2)	9(2)	91(2)
1	0	100	0	100	0	100

[a] experimental values (metal fractions found by elemental analyses)
[b] theoretical values (metal fractions used during the synthesis)

Table S3. Relative contents of Ln and Ln' for $[Tb_{6x}Eu_{6-6x}(3\text{-cb/bb/ib})_{14}]$ complexes with $0 \leq x \leq 1$

	$[Tb_{6x}Eu_{6-6x}(3\text{-cb})_{14}]$		$[Tb_{6x}Eu_{6-6x}(3\text{-bb})_{14}]$		$[Tb_{6x}Eu_{6-6x}(3\text{-ib})_{14}]$	
x^b	Eu^a(%)	Tb^a(%)	Eu^a(%)	Tb^a(%)	Eu^a(%)	Tb^a(%)
0	100	0	100	0	100	0
0.2	81(2)	19(2)	83(2)	17(2)	-	-
0.5	47(2)	53(2)	-	-	50(2)	50(2)
0.7	33(2)	67(2)	32(2)	68(2)	35(2)	65(2)
0.9	11(2)	89(2)	10(2)	90(2)	12(2)	88(2)
0.95	96(2)	4(2)	96(2)	4(2)	94(2)	6(2)
1	0	100	0	100	0	100

[a] experimental values (metal fractions found by elemental analyses)
[b] theoretical values (metal fractions used during the synthesis)

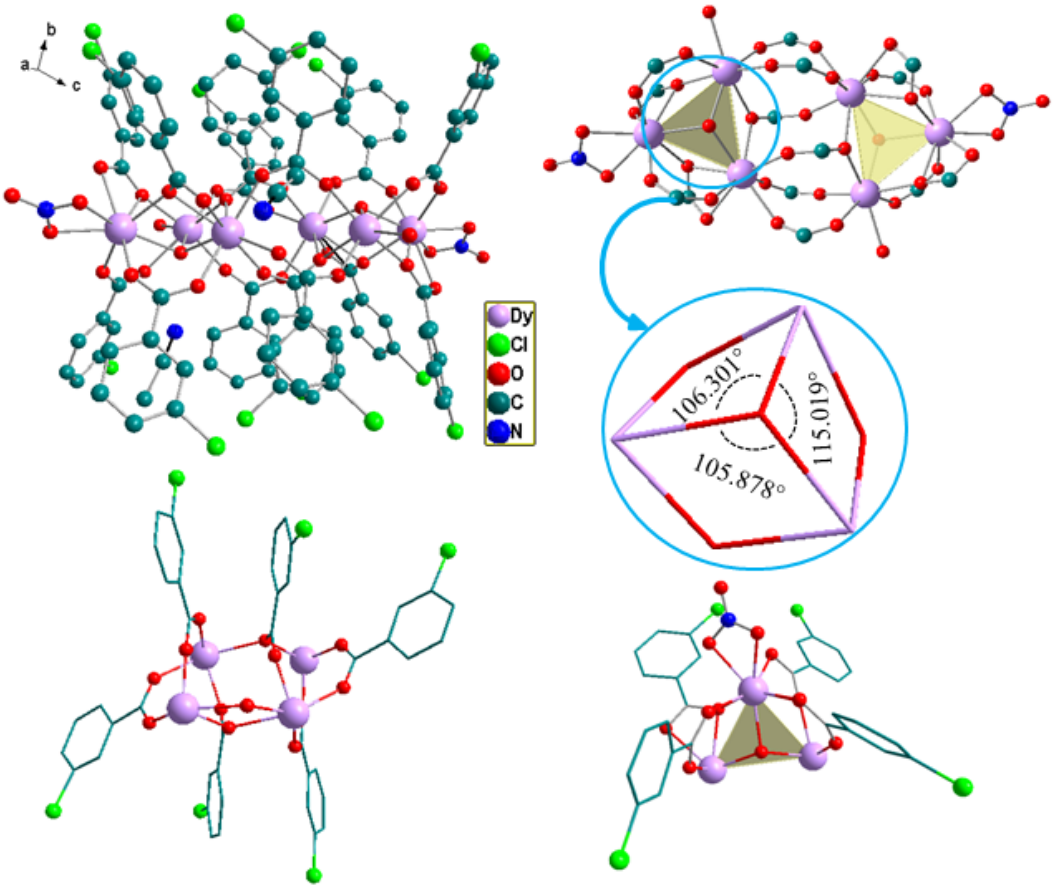

Figure S2. Projection view of the $[Dy_6(3\text{-cb})_{14}]$ (top left). Simplified projection view of the $[Dy_6(3\text{-cb})_{14}]$ where only the carboxylate groups are represented for clarity. In inset, triangular units with the Dy-O-Dy angles (top right). Simplified projection view of a trinuclear triangle (bottom right). Simplified projection view of the linkage of the two triangles (bottom left). In simplified views, only binding ligands have been drawn for clarity. Redrawn from reference 45.

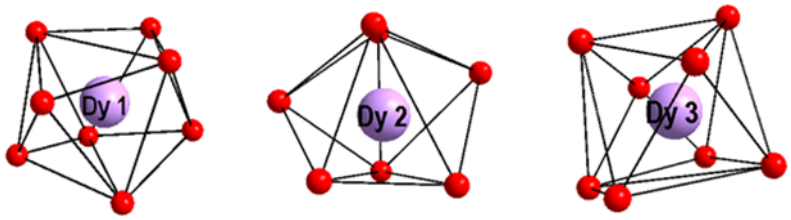

Figure S3. Coordination polyhedra of the three crystallographically independent Dy^{3+} ions in $[Dy_6(3\text{-cb})_{14}]$. Redrawn from reference 45.

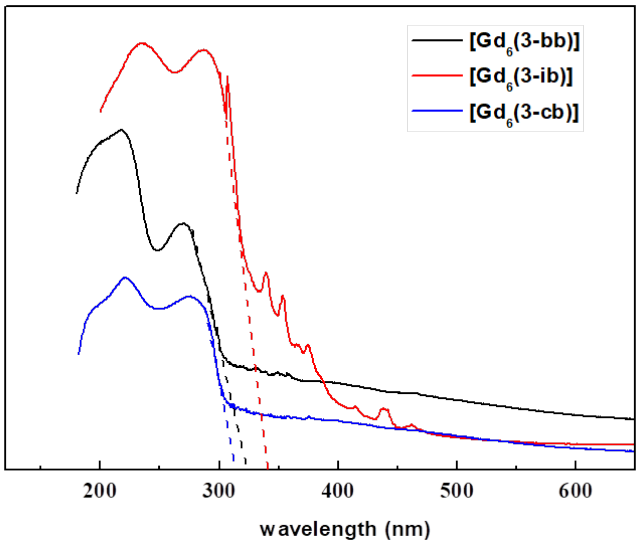

Figure S4. Solid-state UV-vis absorption spectra of $[Gd_6(3\text{-cb})_{14}]$ (blue), $[Gd_6(3\text{-bb})_{14}]$ (black) and $[Gd_6(3\text{-ib})_{14}]$ (red) recorded at room-temperature.

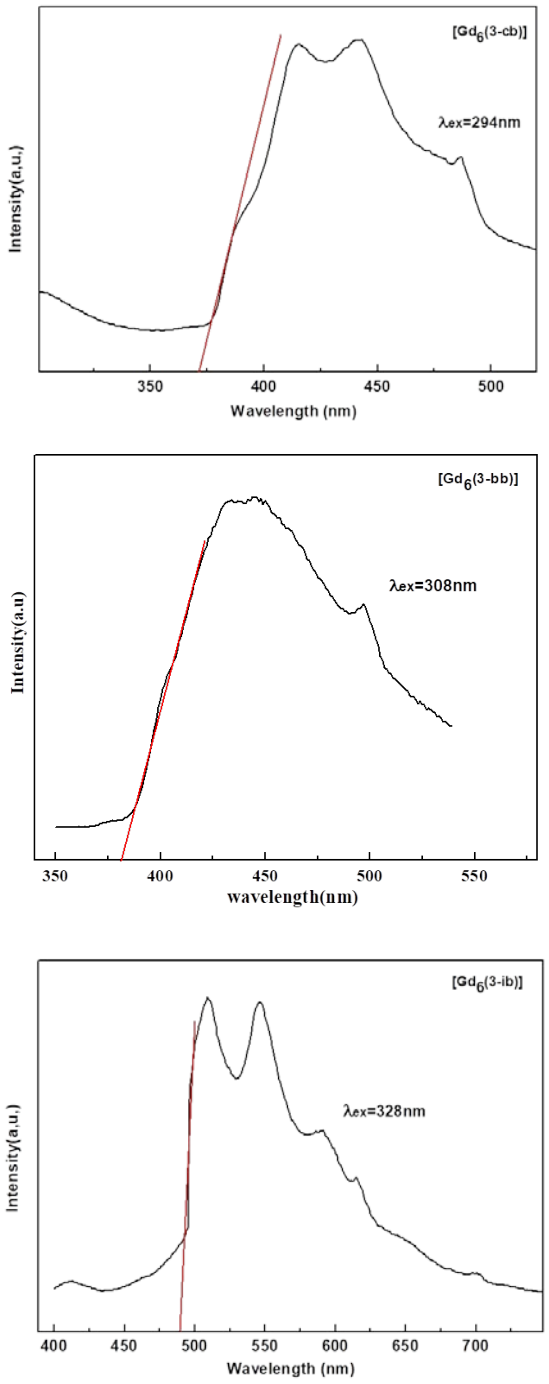

Figure S5. Solid-state emission spectra of $[Gd_6(3\text{-cb})_{14}]$, $[Gd_6(3\text{-bb})_{14}]$ and $[Gd_6(3\text{-ib})_{14}]$ (from top to bottom) recorded at 77K.

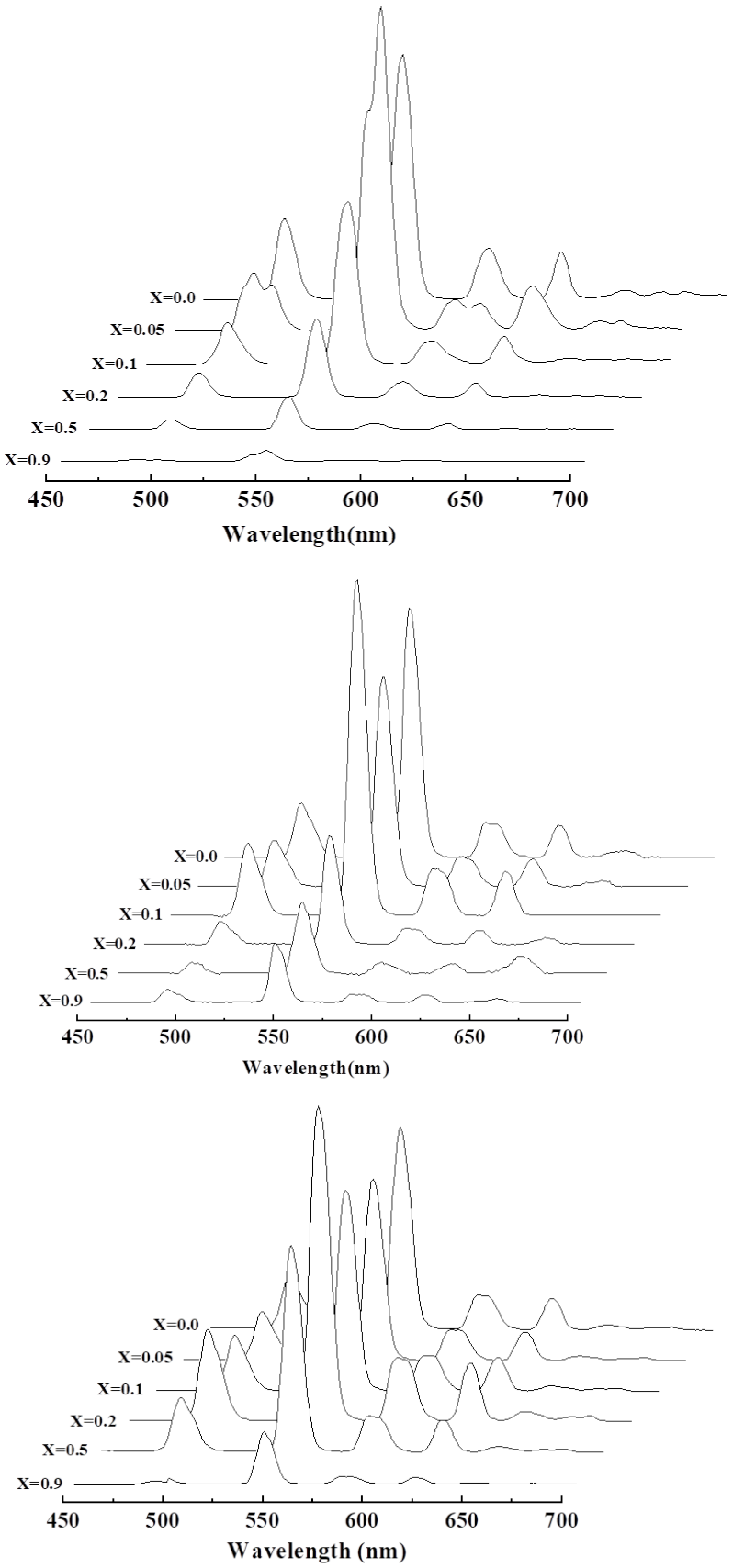

Figure S6. Solid state emission spectra of $[Y_{6x}Tb_{6-6x}(3\text{-cb})_{14}]$ (top), $[Y_{6x}Tb_{6-6x}(3\text{-bb})_{14}]$ (middle) and $[Y_{6x}Tb_{6-6x}(3\text{-ib})_{14}]$ (bottom) *vs x* under 294 nm, 308 nm or 328 nm excitation wavelength, respectively.

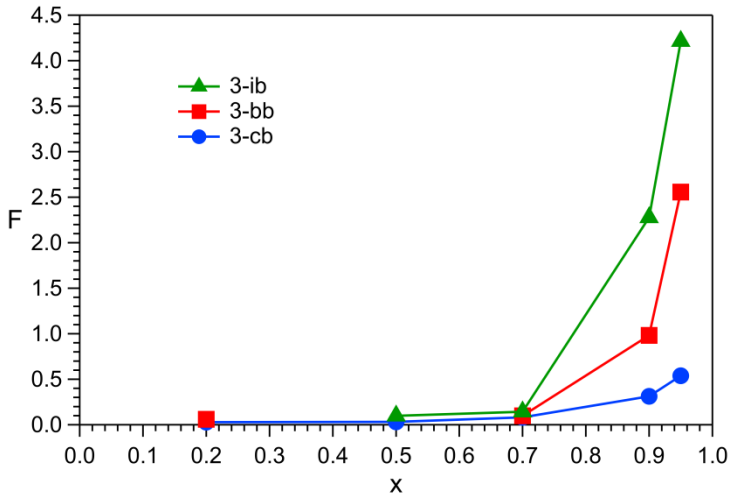

Figure S7. F values *versus* x for $[Tb_{6x}Eu_{6-6x}(3\text{-cb})_{14}]$ (blue curve), $[Tb_{6x}Eu_{6-6x}(3\text{-bb})_{14}]$ (red curve) and $[Tb_{6x}Eu_{6-6x}(3\text{-ib})_{14}]$ (green curve) with $0 \leq x \leq 1$.

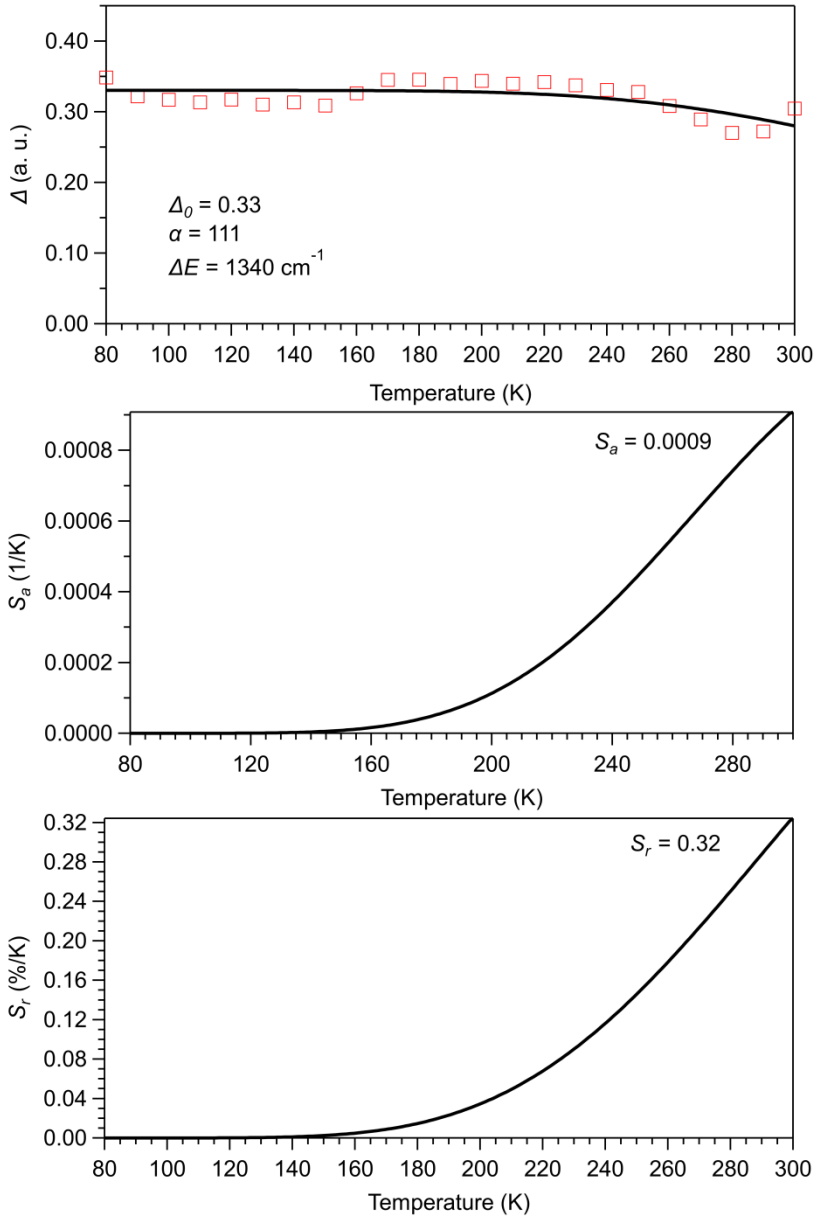

Figure S8. Top: Plot presenting the thermometric parameter vs temperature (K) of $[Tb_4Eu_2(3\text{-cb})_{14}]$ in the solid-state. The red points are the experimental parameter (I_{Tb}/I_{Eu}) and the solid dark line represents the calibration curve obtained by the best fit of the experimental points. Equations used: $\Delta = I_{Tb}/I_{Eu}$ (**1**), $\Delta = \frac{\Delta_0}{1+\alpha\exp(-\frac{\Delta E}{k_B T})}$ (**2**), Δ is the thermometric parameter, I_{Tb} and I_{Eu} are the maximum intensities of the $^5D_4 \rightarrow {}^7F_5$ (Tb^{3+}) and $^5D_0 \rightarrow {}^7F_2$ (Eu^{3+}) transitions, Δ_0 is the thermometric parameter at T = 0 K, $\alpha = \frac{W_0}{W_R}$ is the ratio between the non-radiative (W_0 at T = 0 K) and radiative (W_R) rates, ΔE is the activation energy for the non-radiative channel, and k_B is the Boltzmann constant (= 0.69509 cm^{-1}/K). Middle: Plot presenting S_a values at variable temperature (80 - 300 K) of $[Tb_4Eu_2(3\text{-cb})_{14}]$. Bottom: Plot presenting S_r values at variable temperature (80 - 300 K) of $[Tb_4Eu_2(3\text{-cb})_{14}]$. $S_a = \left|\frac{\partial \Delta}{\partial T}\right|$ (**3**) and $S_r = 100\% \times \left|\frac{1}{\Delta}\frac{\partial \Delta}{\partial T}\right|$ (**4**), S_a et S_r are the absolute and relative temperature sensitivities.

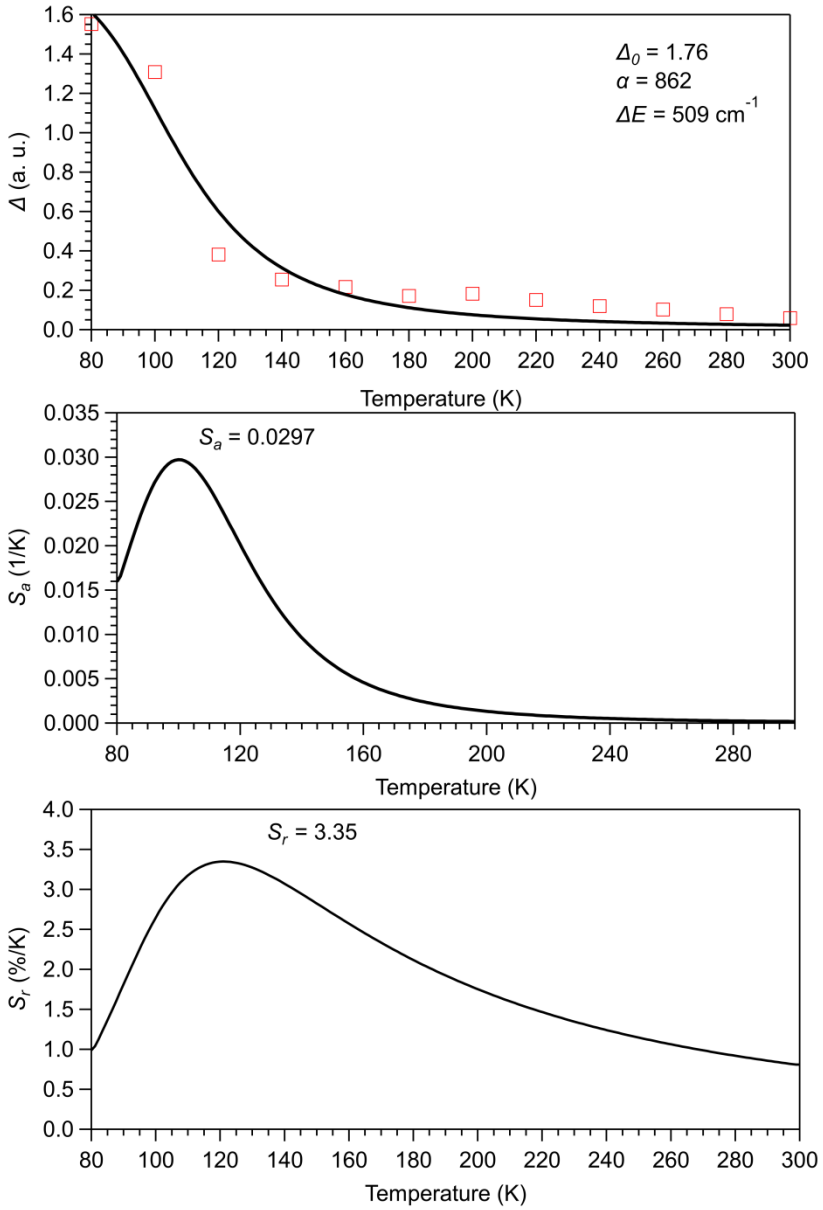

Figure S9. Top: Plot presenting the thermometric parameter vs temperature (K) of $[Tb_4Eu_2(3\text{-bb})_{14}]$ in the solid-state. The red points are the experimental parameter (I_{Tb}/I_{Eu}) and the solid dark line represents the calibration curve obtained by the best fit of the experimental points. Equations used: $\Delta = I_{Tb}/I_{Eu}$ (**1**), $\Delta = \frac{\Delta_0}{1+\alpha\exp(-\frac{\Delta E}{k_B T})}$ (**2**), Δ is the thermometric parameter, I_{Tb} and I_{Eu} are the maximum intensities of the $^5D_4 \rightarrow {}^7F_5$ (Tb^{3+}) and $^5D_0 \rightarrow {}^7F_2$ (Eu^{3+}) transitions, Δ_0 is the thermometric parameter at T = 0 K, $\alpha = \frac{W_0}{W_R}$ is the ratio between the non-radiative (W_0 at T = 0 K) and radiative (W_R) rates, ΔE is the activation energy for the non-radiative channel, and k_B is the Boltzmann constant (= 0.69509 cm^{-1}/K). Middle: Plot presenting S_a values at variable temperature (80 - 300 K) of $[Tb_4Eu_2(3\text{-bb})_{14}]$. Bottom: Plot presenting S_r values at variable temperature (80 - 300 K) of $[Tb_4Eu_2(3\text{-bb})_{14}]$. $S_a = \left|\frac{\partial \Delta}{\partial T}\right|$ (**3**) and $S_r = 100\% \times \left|\frac{1}{\Delta}\frac{\partial \Delta}{\partial T}\right|$ (**4**), S_a et S_r are the absolute and relative temperature sensitivities.

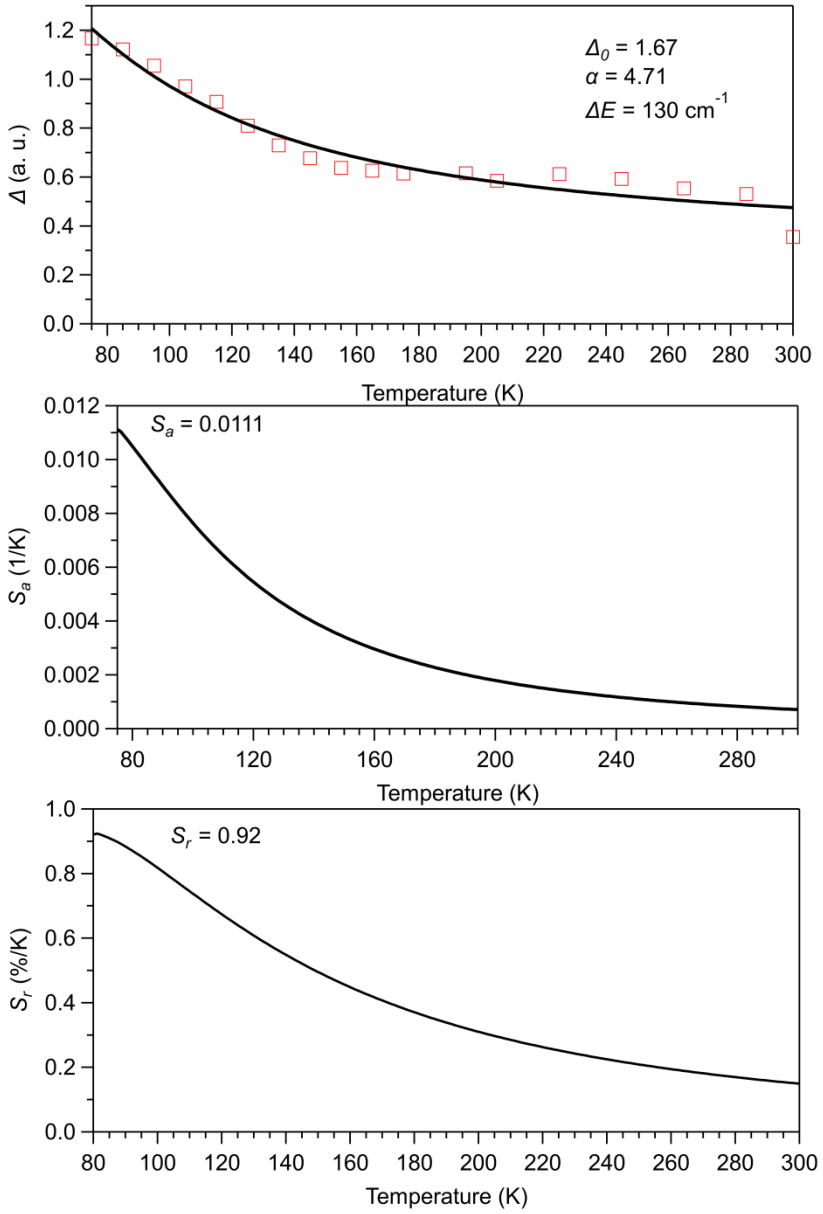

Figure S10. Top: Plot presenting the thermometric parameter vs temperature (K) of $[Tb_4Eu_2(3\text{-ib})_{14}]$ in the solid-state. The red points are the experimental parameter (I_{Tb}/I_{Eu}) and the solid dark line represents the calibration curve obtained by the best fit of the experimental points. Equations used: $\Delta = I_{Tb}/I_{Eu}$ (**1**), $\Delta = \frac{\Delta_0}{1+\alpha\exp(-\frac{\Delta E}{k_B T})}$ (**2**), Δ is the thermometric parameter, I_{Tb} and I_{Eu} are the maximum intensities of the $^5D_4 \rightarrow {}^7F_5$ (Tb^{3+}) and $^5D_0 \rightarrow {}^7F_2$ (Eu^{3+}) transitions, Δ_0 is the thermometric parameter at T = 0 K, $\alpha = \frac{W_0}{W_R}$ is the ratio between the non-radiative (W_0 at T = 0 K) and radiative (W_R) rates, ΔE is the activation energy for the non-radiative channel, and k_B is the Boltzmann constant (= 0.69509 cm^{-1}/K). Middle: Plot presenting S_a values at variable temperature (80 - 300 K) of $[Tb_4Eu_2(3\text{-ib})_{14}]$. Bottom: Plot presenting S_r values at variable temperature (80 - 300 K) of $[Tb_4Eu_2(3\text{-ib})_{14}]$. $S_a = \left|\frac{\partial \Delta}{\partial T}\right|$ (**3**) and $S_r = 100\% \times \left|\frac{1}{\Delta}\frac{\partial \Delta}{\partial T}\right|$ (**4**), S_a et S_r are the absolute and relative temperature sensitivities.

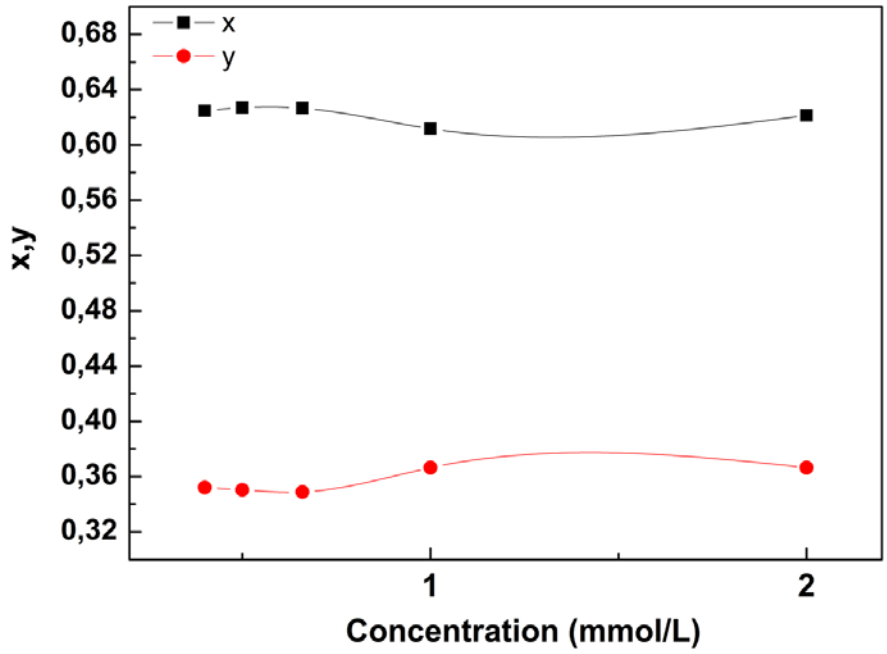

Figure S11. Colorimetric coordinates of hexane solutions of $[Eu_3Tb_3(3\text{-cb})_{14}]$ *vs* concentration (C_0 to $C_0/5$).

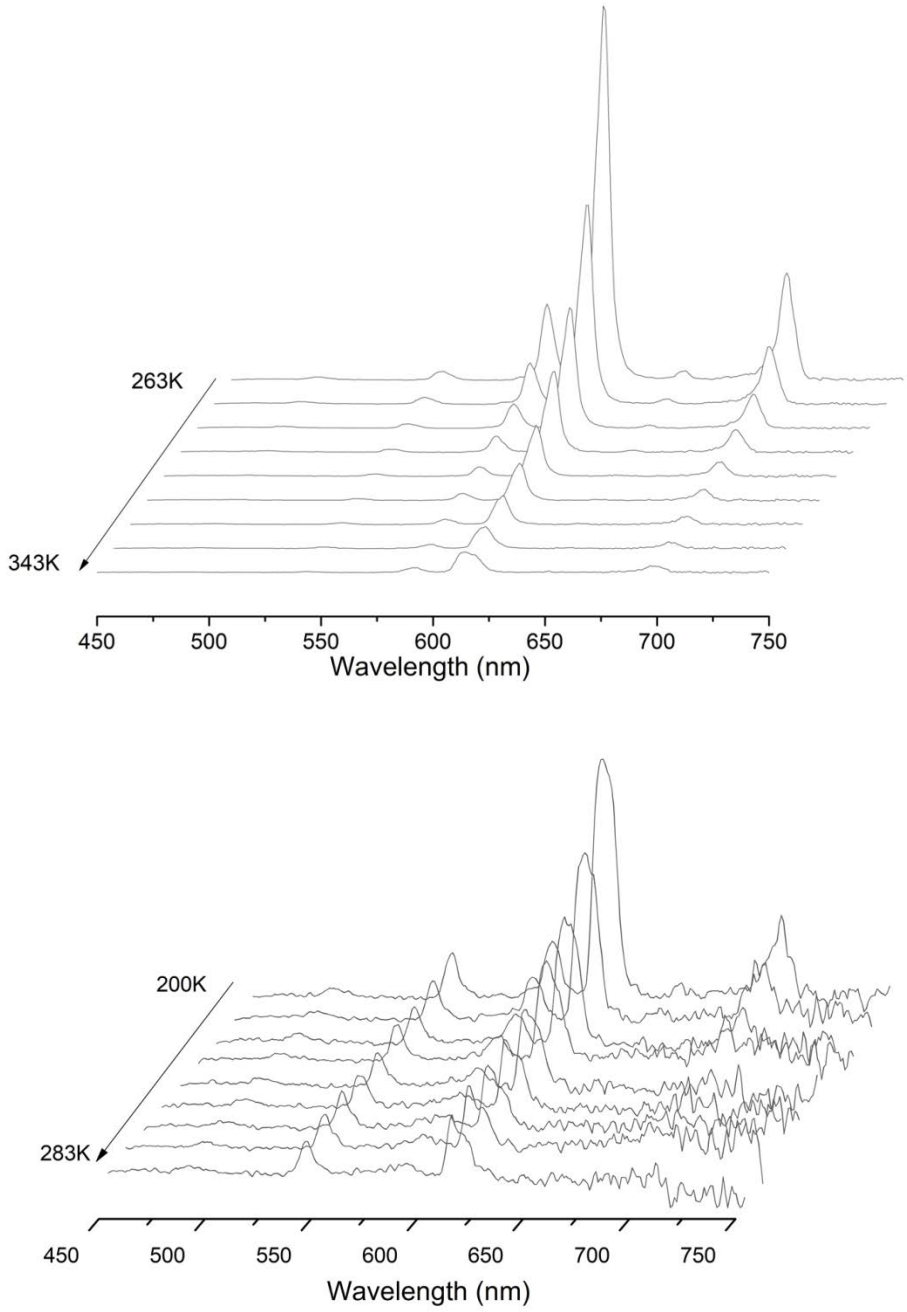

Figure S12. Emission spectra *vs* temperature of a $[Tb_4Eu_2(3\text{-ib})_{14}]$ solution in heptane ($C_0 = 2.10^{-3}$ mol.L^{-1}) between 263 K and 343 K (top) and between 200 K and 283 K (bottom). Both series of spectra have been recorded with different setups which explain the different sensitivities.

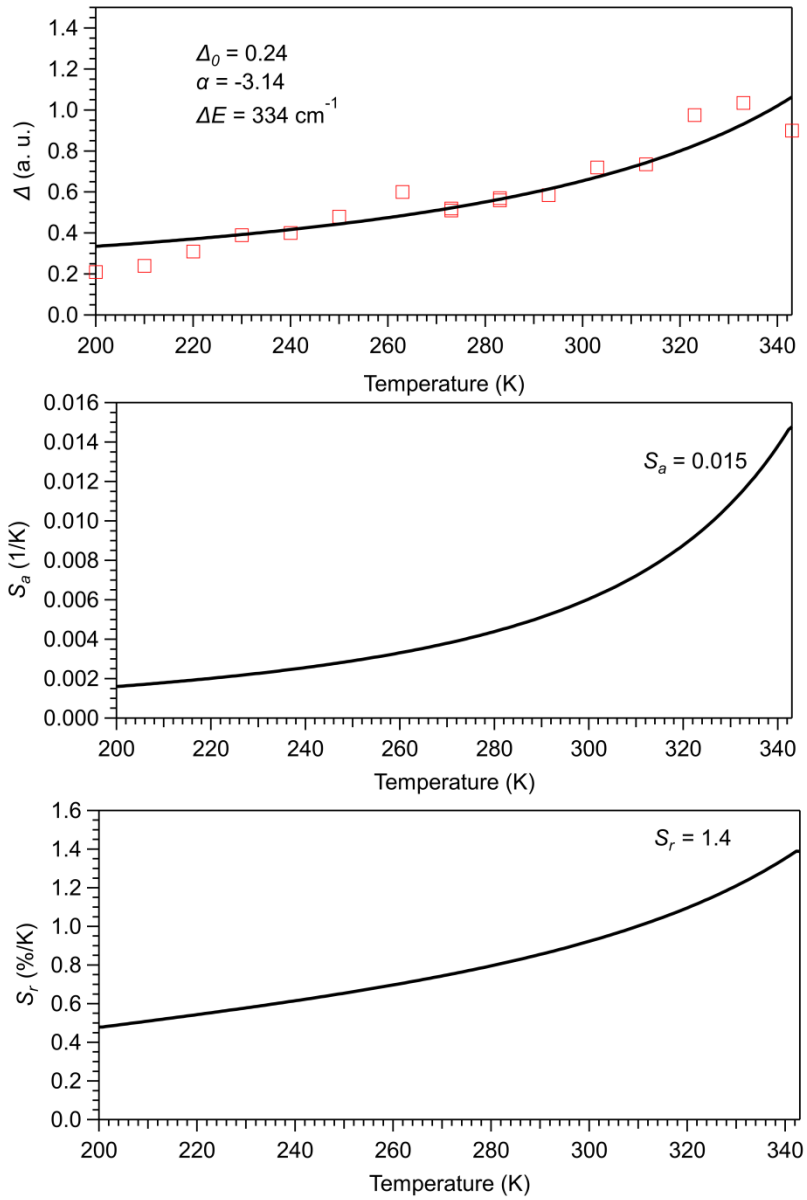

Figure S13. Top: Plot presenting the thermometric parameter *vs* temperature (K) of $[Tb_4Eu_2(3\text{-ib})_{14}]$ in heptane solution. The red points are the experimental parameter (I_{Tb}/I_{Eu}) and the solid dark line represents the calibration curve obtained by the best fit of the experimental points. Equations used: $\Delta = I_{Tb}/I_{Eu}$ (**1**), $\Delta = \frac{\Delta_0}{1+\alpha\exp(-\frac{\Delta E}{k_B T})}$ (**2**), Δ is the thermometric parameter, I_{Tb} and I_{Eu} are the maximum intensities of the $^5D_4 \rightarrow {}^7F_5$ (Tb^{3+}) and $^5D_0 \rightarrow {}^7F_2$ (Eu^{3+}) transitions, Δ_0 is the thermometric parameter at T = 0 K, $\alpha = \frac{W_0}{W_R}$ is the ratio between the non-radiative (W_0 at T = 0 K) and radiative (W_R) rates, ΔE is the activation energy for the non-radiative channel, and k_B is the Boltzmann constant (= 0.69509 cm^{-1}/K). Middle: Plot presenting S_a values at variable temperature (80 - 300 K) of $[Tb_4Eu_2(3\text{-ib})_{14}]$ in heptane solution. Bottom: Plot presenting S_r values at variable temperature (80 - 300 K) of $[Tb_4Eu_2(3\text{-ib})_{14}]$ in heptane solution. $S_a = \left|\frac{\partial \Delta}{\partial T}\right|$ (**3**) and $S_r = 100\% \times \left|\frac{1}{\Delta}\frac{\partial \Delta}{\partial T}\right|$ (**4**), S_a et S_r are the absolute and relative temperature sensitivities.